Structure of crystallized particles in sputter-deposited amorphous germanium films

doi: 10.1107/S1600576718012153

JOURNAL OF APPLIED CRYSTALLOGRAPHY

ISSN: 1600-5767
journals.iucr.org/j

Structure of crystallized particles in sputter-deposited amorphous germanium films

Masayuki Okugawa, Ryusuke Nakamura, Akihiko Hirata, Manabu Ishimaru, Hidehiro Yasuda and Hiroshi Numakura

J. Appl. Cryst. (2018). **51**, 1467–1473

JOURNAL OF APPLIED CRYSTALLOGRAPHY

ISSN 1600-5767

Received 14 June 2018
Accepted 28 August 2018

Edited by V. Holý, Charles University, Prague, Czech Republic and CEITEC at Masaryk University, Brno, Czech Republic

Keywords: crystallized Ge thin films; twinning; streaking effects.

Structure of crystallized particles in sputter-deposited amorphous germanium films

Masayuki Okugawa,[a] Ryusuke Nakamura,[a]* Akihiko Hirata,[b] Manabu Ishimaru,[c] Hidehiro Yasuda[d] and Hiroshi Numakura[a]

[a]Department of Materials Science, Osaka Prefecture University, Naka-ku Gakuen-cho 1-1, Sakai, Osaka 599-8531, Japan, [b]Graduate School of Fundamental Science and Engineering, Waseda University, Okubo 3-4-1, Shinjuku, Tokyo 169-8555, Japan, [c]Department of Materials Science and Engineering, Kyushu Institute of Technology, Tobata Sensui-cho 1-1, Kitakyushu, Fukuoka 804-8550, Japan, and [d]Research Center for Ultra-High Voltage Electron Microscopy, Osaka University, Mihogaoka 7-1, Ibaraki, Osaka 567-0047, Japan. *Correspondence e-mail: nakamura@mtr.osakafu-u.ac.jp

Pristine thin films of amorphous Ge prepared by sputtering are unstable and form coarse crystalline particles of 100 nm in size upon crystallization by electron irradiation. These crystalline particles exhibit unusual diffraction patterns that cannot be understood from the diamond cubic structure. The structure has previously been assumed to be a metastable hexagonal form. In the present work, the structure of the coarse crystalline particles has been analysed in detail by transmission electron microscopy, considering the possibility that those diffraction patterns might occur with the diamond cubic structure if the particle consists of thin twin layers. By high-resolution lattice imaging the particles have been shown to be of the diamond cubic structure containing a high density of twins and stacking faults parallel to {111}. With such defects, diffraction patterns can be complex because of the following effects: superposition of two or more diffraction patterns of the same structure but of different orientations, double diffraction through twin crystals, and streaks parallel to the thin crystal which give rise to extra diffraction spots. It is found that diffraction patterns taken from various orientations can be explained in terms of these effects.

1. Introduction

Thin films of silicon and germanium are technologically very important in the electronics and opto-electronics industries in applications such as solar cells, thin-film transistors *etc.* (Poate & Mayer, 1982; Matsuda, 2004). Developments in their process technology are being made to further reduce the film thickness, thereby achieving higher efficiency. Since poly-crystalline films are produced by rapid annealing of amorphous films, a detailed understanding of the crystallization process is essential for the synthesis. It is assumed that crystallization behaviour depends largely on the initial amorphous structure. From both scientific and technological perspectives, therefore, it is interesting and important to clarify progressive changes of structure from prepared amorphous states to terminal crystalline phases.

We have recently reported the relationship between the structure of amorphous germanium (a-Ge) films prepared by sputtering and their crystallization behaviour (Okugawa *et al.*, 2016*a*,*b*,*c*). Sputter-deposited a-Ge films are initially unstable and are stabilized by ageing at room temperature (Okugawa *et al.*, 2016*a*), thermal treatment (Okugawa *et al.*, 2016*c*) and low-flux electron irradiation (Okugawa *et al.*, 2016*b*). Unstable a-Ge crystallizes inhomogeneously to coarse crystalline particles of 100–200 nm in diameter, whereas stabilized a-Ge

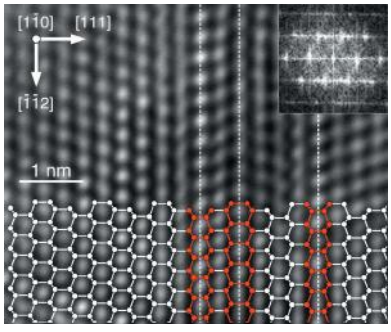

crystallizes homogeneously to fine nanograins. Electron diffraction experiments (Okugawa *et al.*, 2016*b*) indicated that the fine nanograins were of the diamond cubic structure. On the other hand, the structure of the crystalline particles was found to be non-cubic: the diffraction spots located at positions close to the {111} interplanar distance of the diamond cubic structure have interplanar angles of 56 and 62°, neither of which exists in the cubic structure, in which {111} plane normals make angles of 71 or 109°. The unusual 56°-type diffraction pattern was originally reported by Parsons & Hoelke (1983) for crystallized regions in a-Ge films prepared by vapour deposition. In addition, they observed another puzzling diffraction pattern in which diffraction spots appear at the {111} interplanar distance with sixfold symmetry (Parsons & Hoelke, 1985). From those observations, they concluded that the structure of the crystalline phase was hexagonal with the cell parameters a = 3.96 Å and c = 9.80 Å (c/a = 2.47), although the detailed atomic arrangement was unknown. In our previous report (Okugawa *et al.*, 2016*b*), we came to the same conclusion as Parsons & Hoelke (1983, 1985), that the crystal structure of the crystalline particle was hexagonal, but further analysis was necessary to determine the structure.

We have recently come to notice that the 56°-type diffraction pattern could be explained by superposition of multiple diffraction patterns from differently oriented cubic crystallites. This idea was originally proposed by Dickson & Pashley (1962) for gold and silver layers deposited on mica. Buffat *et al.* (1991) analysed gold nanoparticles by high-resolution transmission electron microscopy (TEM), and showed that the 56°-type diffraction pattern was due to superposition of twinned face-centred cubic crystallites. Kohno *et al.* (2003) found the 56°-type diffraction pattern from Si nanoparticles and confirmed that it could occur from {111} twinned diamond cubic crystals. In addition, they found that the diffraction spots of sixfold symmetry corresponding to the {111} spacing could be explained by elongation of diffraction spots caused by thin twins, which they refer to as a 'truncation effect'. Cayron, den Hertog and their co-workers (Cayron *et al.*, 2009; den Hertog *et al.*, 2012) examined these unusual diffraction patterns of Si nanowires and films in terms of a hexagonal and {111} twinned diamond cubic structure, and also concluded that the diffraction patterns were due to the twinning effects. In this study, we have re-analysed the structure of the crystalline particles that appear in the unstable a-Ge matrix by considering these possibilities. Atomic arrangements in the crystalline particles were examined by high-resolution TEM, and diffraction patterns of a crystalline particle from various orientations were analysed to determine the space group. The structure of the crystalline particles turns out to be not hexagonal but cubic, including planar defects parallel to {111}.

2. Experimental procedure

Thin films of amorphous Ge with a thickness of 40 nm were prepared by radio-frequency (RF) sputtering. The films were deposited on a cleaved rock salt crystal at the ambient temperature under an RF output power of 50 W and an argon pressure of 0.7 Pa. The film and the substrate were put into distilled water, and then the floating film was recovered on a molybdenum grid.

An as-deposited sample aged for a few days after the deposition was irradiated with electrons at a high flux above 1.3×10^{23} m^{-2} s^{-1} in a transmission electron microscope operating at 125 kV (Hitachi H-7000), by which means coarse crystalline particles with a 'metastable' structure were formed (Okugawa *et al.*, 2016*a*). Selected-area electron diffraction (SAED) patterns and high-resolution images of the crystalline particles were observed by conventional TEM (JEOL 2000FX and Hitachi HF2000 instruments). To avoid contamination, all the TEM experiments were performed with a liquid-nitrogen cold trap placed close to the sample holder.

3. Results and discussion

3.1. Atomic structure of coarse crystalline particles

Fig. 1(*a*) shows a region irradiated with an electron beam with a flux of 1.3×10^{23} m^{-2} s^{-1} for a few seconds. The beam

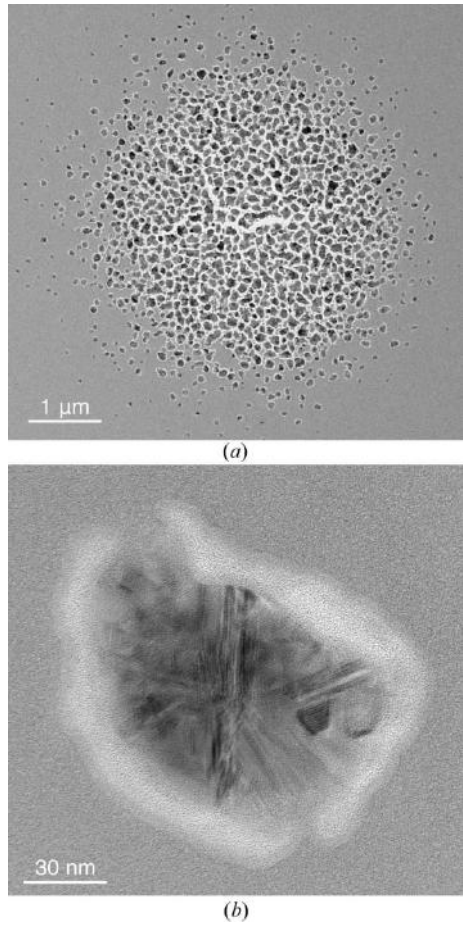

Figure 1
(*a*) A bright-field image of a region crystallized by electron irradiation of an a-Ge film aged for a few days after sputter deposition. The energy and the flux of the electron beam were 125 keV and 1.3×10^{23} m^{-2} s^{-1}, respectively. (*b*) A magnified image of a typical crystalline particle.

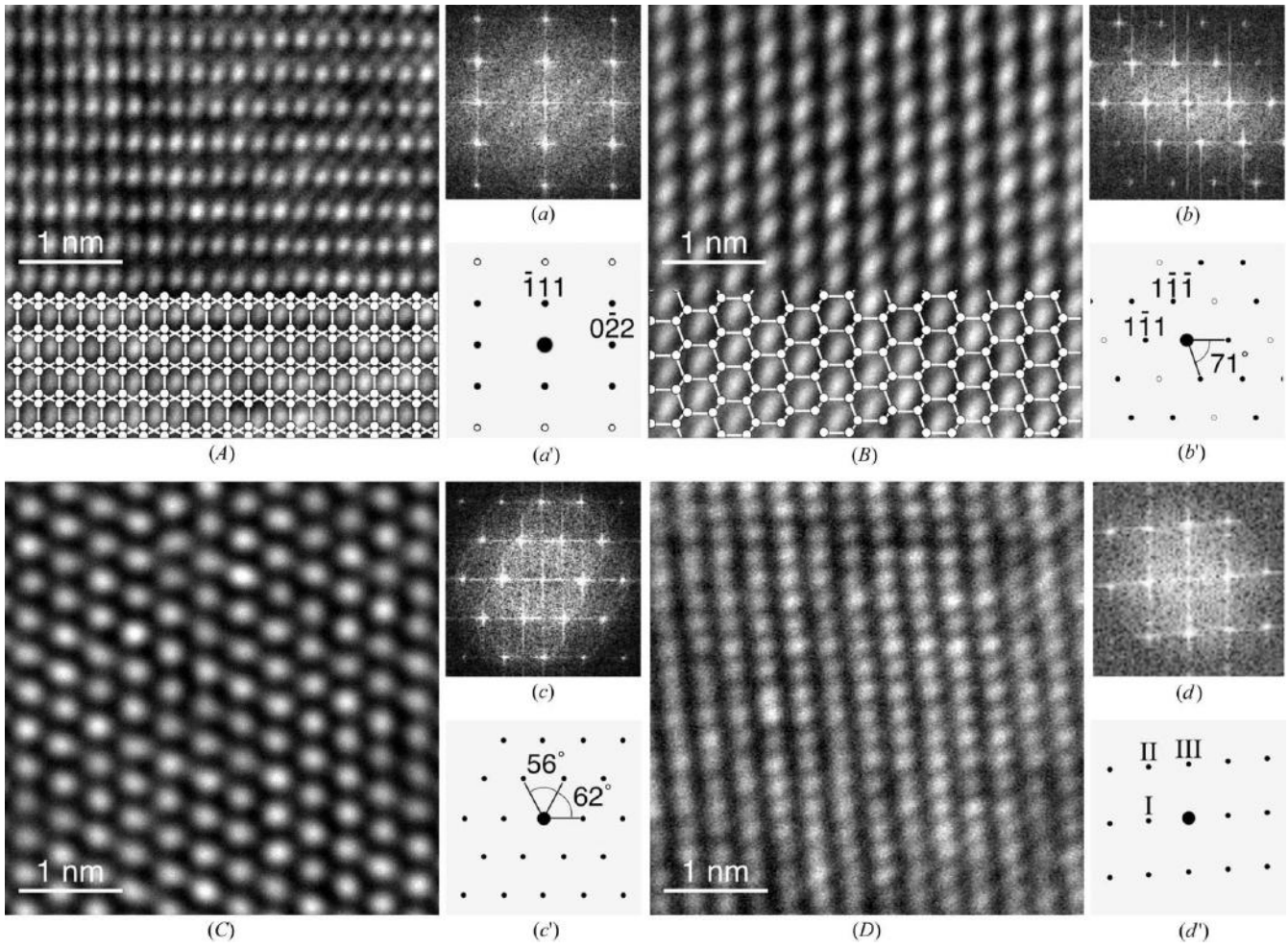

Figure 2
(*A*)–(*D*) High-resolution TEM images of crystalline particles and (*a*)–(*d*) their Fourier power spectra. (*a*′), (*b*′) Simulated electron diffraction patterns of the diamond cubic structure from [211] and [110]. (*c*′), (*d*′) Illustrations of the Fourier spectra of (*c*) and (*d*).

diameter was about 1 µm. Coarse crystalline particles of 100–200 nm in diameter, appearing in dark contrast, formed radially around the centre of the electron beam. Fig. 1(*b*) shows a magnified image of a typical coarse crystalline particle, which includes a number of planar defects.

The atomic structures of such crystalline particles were examined by high-resolution TEM. Fig. 2 shows high-resolution TEM images and their Fourier power spectra of nondefective parts of crystalline particles. The first two sets of images and Fourier spectra (Figs. 2*A*, 2*a* and 2*B*, 2*b*) can be understood by assuming a cubic structure with the incident beam parallel to [211] and [110], respectively. Simulated diffraction patterns are shown in Figs. 2(*a*′) and 2(*b*′), and the atomic arrangements are displayed on the TEM image. These are in good agreement with the observed images. The other two sets (Figs. 2*C*, 2*c* and 2*D*, 2*d*) are examples that cannot apparently be accounted for in terms of the diamond cubic structure. The lattice image of Fig. 2(*C*) appears to have sixfold symmetry at first glance but it actually does not. The Fourier spectrum of Fig. 2(*c*) is essentially the same as those reported in the literature by other authors (Dickson & Pashley, 1962; Parsons & Hoelke, 1983; Buffat *et al.*, 1991; Kohno *et al.*, 2003; Cayron

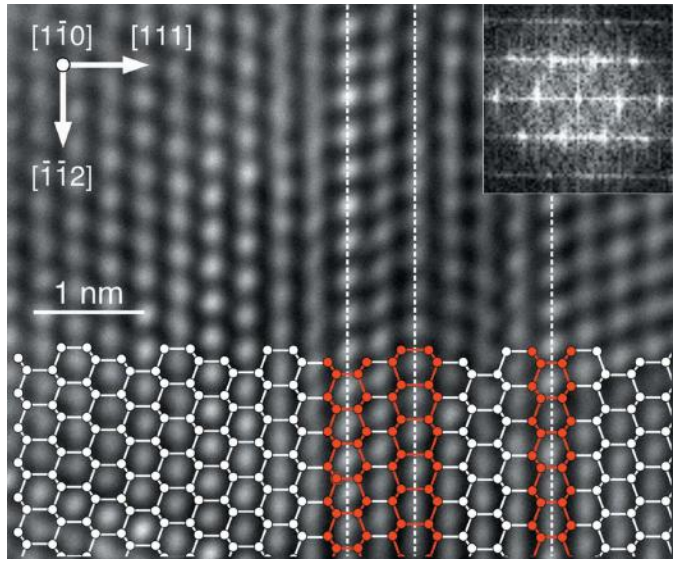

Figure 3
A high-resolution bright-field image and a corresponding Fourier spectrum from [1$\bar{1}$0] of the diamond cubic structure. An atomic model is superimposed at the bottom of the image. The three dashed lines indicate (111) stacking faults.

et al., 2009; den Hertog *et al.*, 2012) and recently by the present authors, as mentioned in the *Introduction*; the six nearest spots appear at the distance corresponding to the {111} spacing but none of the angles between them is exactly 60°, as indicated in Fig. 2(*c*′). The Fourier power spectrum of Fig. 2(*d*) is illustrated in Fig. 2(*d*′), in which the prominent spots are labelled I, II and III. The distances to spots I and II are close to those of 111 and 220 of the diamond cubic structure, but the angle between them, which is about 57°, is not close to any of the possible values (35, 90 and 145°). In addition, spot III, which appears at a distance between those of I and II, cannot occur with the diamond cubic structure; there must be no reflection planes between {111} and {220}.

Fig. 3 shows a high-resolution TEM image of a defective part of a coarse crystalline particle and its Fourier spectrum. The direction of observation is parallel to [1$\bar{1}$0] of the assumed diamond cubic structure. This image can be interpreted as a projection of the diamond cubic structure with planar defects parallel to (111) planes (indicated by white dashed lines); the atomic arrangement is illustrated in the lower part. The defects are very thin twins containing less than ten (111) planes. Such a defective structure is similar to the model assumed for Si nanoparticles by Kohno *et al.* (2003) and for Si nanowires and Si films by Cayron *et al.* (2009).

3.2. Diffraction patterns of coarse crystalline particles

To identify the space group, a single-crystalline particle of 100 nm in diameter in the amorphous matrix was examined in detail by taking SAED patterns from various directions by rotating the sample. The aperture diameter was approximately 200 nm, so that both the diffraction spots from the crystalline particle and the halo rings from the amorphous matrix are present in the patterns. In Fig. 4(*a*1), the strong diffraction

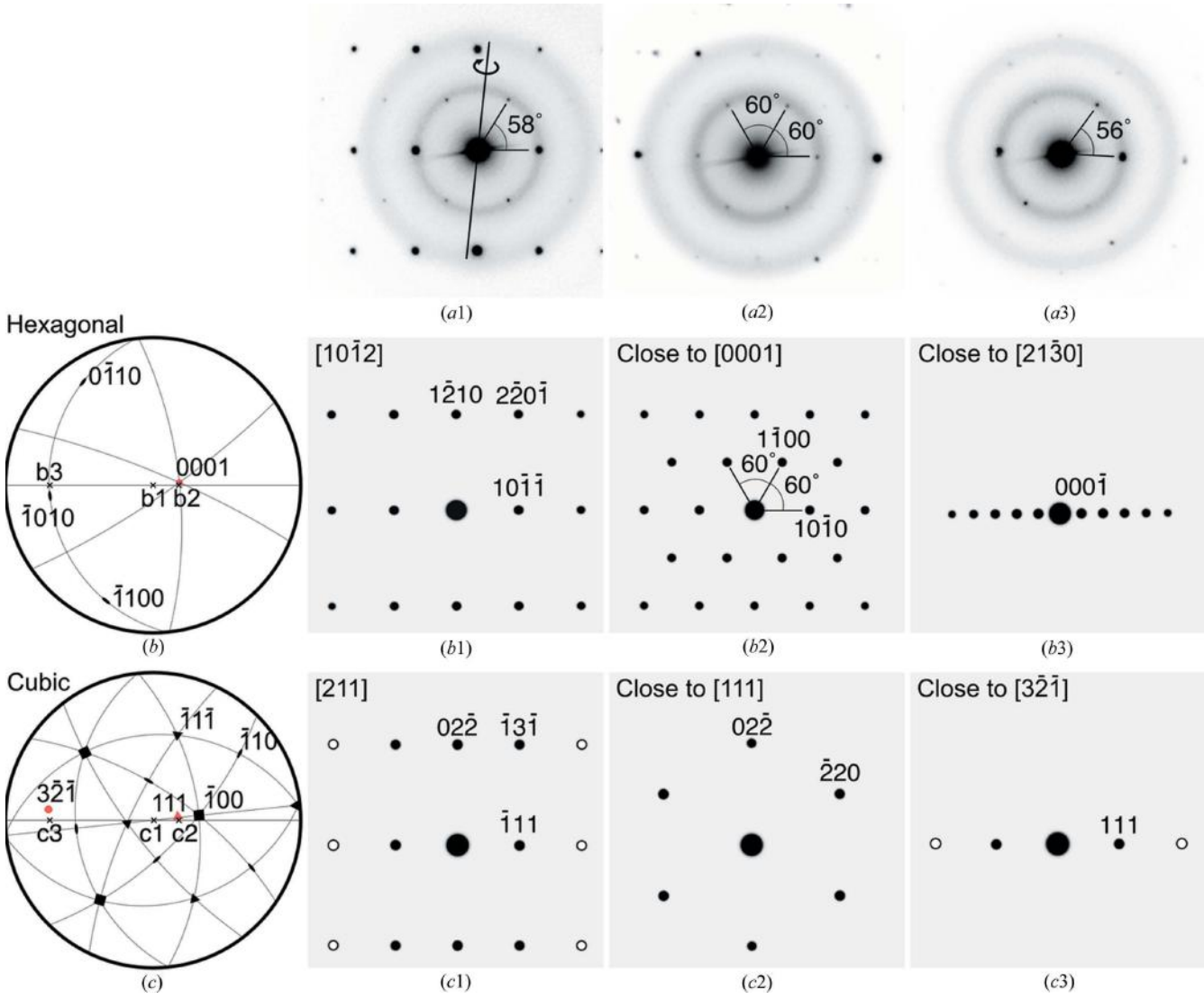

Figure 4
(*a*1)–(*a*3) Electron diffraction patterns taken from a coarse crystallized particle at a tilt angle of 0° (*a*1), +20° (*a*2) and −70° (*a*3). Simulated diffraction patterns of a hexagonal structure from the [10$\bar{1}$2] direction (*b*1) and the diamond cubic structure from the [211] direction (*c*1). The tilt angle of (*b*2) and (*c*2) is +20°, and that of (*b*3) and (*c*3) is −70°. Filled and open circles indicate fundamental and double diffraction spots, respectively. (*b*), (*c*) Stereographic projections of the hexagonal and the cubic structure.

spots above and below the direct beam make a right angle with those to the sides of the direct beam. In Fig. 4(*a*2), which was taken after rotating the sample by +20° about the axis shown in Fig. 4(*a*1), diffraction spots appear at every 60° on the first and the second halo rings. Fig. 4(*a*3) is the pattern taken at −70° from the original orientation of Fig. 4(*a*1). Diffraction spots appear at positions close to the first halo ring with an interplanar angle of 56°.

In order to understand the observed diffraction patterns, theoretical patterns were calculated for two models, a hexagonal structure (Figs. 4*b*1–4*b*3) and the diamond cubic structure (Figs. 4*c*1–4*c*3), both of which have strong diffraction spots that constitute the same orthogonal pattern as in Fig. 4(*a*1). Space group *P*6 was chosen for the hexagonal structure, with the lattice parameters a = 3.80 Å and c = 9.16 Å, and a Ge atom at the origin in the unit cell. Diffraction patterns from various orientations on the solid curves in the stereographic projection (Fig. 4*b*) were simulated. Fig. 4(*b*1) is the diffraction pattern from [10$\bar{1}$2]. Turning the incident beam direction to +20° (*b*2), which is close to [0001], the diffraction spots 1$\bar{1}$00 and 10$\bar{1}$0, which make angles of 60°, appear at the same positions as in Fig. 4(*a*2). On the other hand, the diffraction pattern at −70° (*b*3) is completely different from Fig. 4(*a*3). In the case of the diamond cubic structure, the strong spots of Fig. 4(*a*1) can be consistent with the diffraction pattern from [211] (Fig. 4*c*1), if double-diffraction effects are considered, as indicated by open circles in Fig. 4(*c*1). At the incident beam direction of +20° from the original orientation along the solid curve in the stereographic projection (Fig. 4*c*), the diffraction pattern from [111] appears, as shown in Fig. 4(*c*2). Diffraction spots of the 220 family of sixfold symmetry appear on the second halo ring, but the spots on the first halo ring observed in the experiment (Fig. 4*a*2) are absent. At the direction of −70°, which is close to [3$\bar{2}\bar{1}$] (Fig. 4*c*3), diffraction spots corresponding to 111 and $\bar{1}\bar{1}\bar{1}$ appear in the diffraction pattern. These SAED patterns can be explained neither by a hexagonal nor by the diamond cubic structure.

3.3. Simulated diffraction patterns of defective particles of the diamond cubic structure

Following Kohno *et al.* (2003) and Cayron *et al.* (2009), we consider a defective crystallite of the diamond cubic structure which contains thin (111) twins. In this case, electron diffraction patterns can be a superposition of patterns from different orientations, and streaks can appear in the direction perpendicular to the twins.

Fig. 5(*a*) shows a projection of the atomic arrangement in a set of twin crystals, parallel to [312] of one domain (atom positions indicated by black circles) and to [132] of the other (red circles). Both [312] and [132] directions make angles of 22° with the (111) plane normal.

Each domain produces independently fundamental diffraction spots of 111 type, indicated by filled circles in black and red which make angles of 56° (Fig. 5*a*1). Double diffraction spots of 222 type also appear, as shown by open circles in black and red. In addition, double diffraction of electrons passing through the two twin crystallites brings about the extra spots shown by open squares in Fig. 5(*a*2). The original and double diffraction spots have an interplanar angle of 62°. This diffraction pattern agrees well with Fig. 4(*a*3). The atomic arrangement (Fig. 5*a*) is also consistent with the experimental

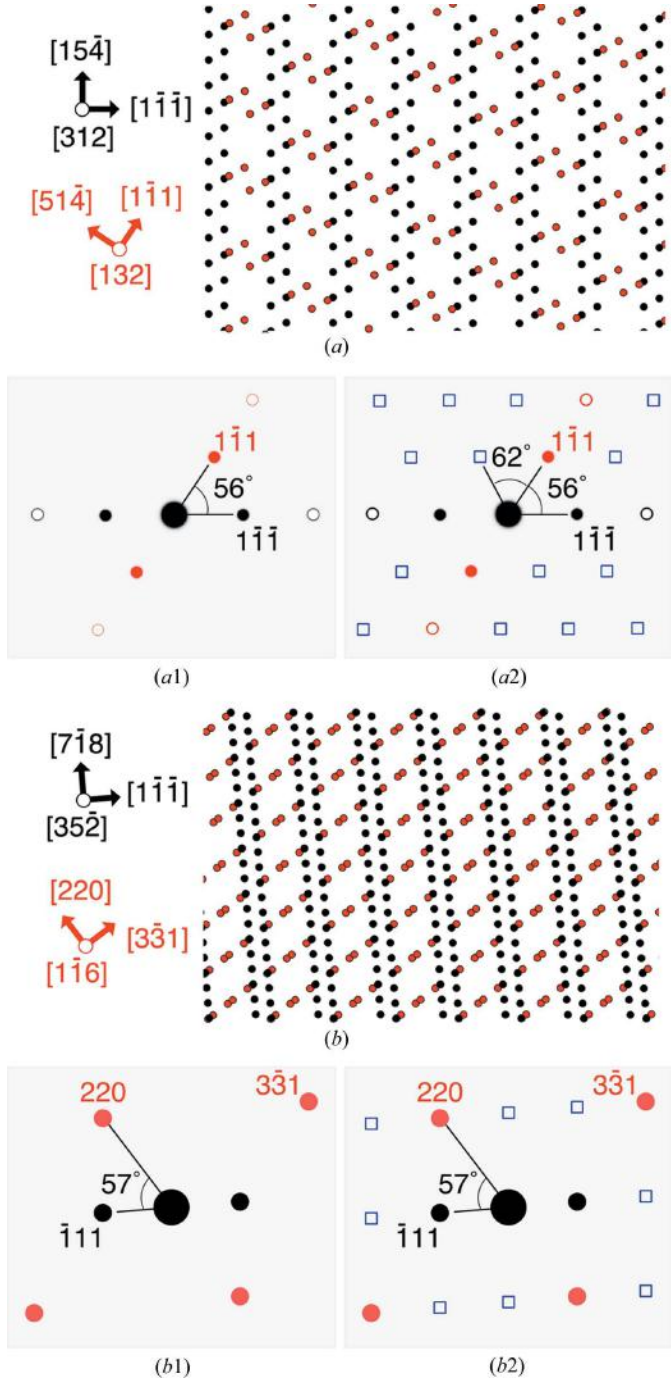

Figure 5
(*a*), (*b*) (111) twinned diamond cubic structures, and (*a*1), (*a*2), (*b*1), (*b*2) corresponding electron diffraction patterns. The direction of observation is parallel to [312] and [132] (*a*), (*a*1), (*a*2) and to [35$\bar{2}$ and [1$\bar{1}$6] (*b*), (*b*1), (*b*2). (*a*1), (*b*1) Superposition of the diffraction patterns from each domain. (*a*2), (*b*2) The same patterns as (*a*1), (*b*1) but with extra spots (blue) caused by double diffraction through the twin layers.

lattice image (Fig. 2*C*). The high-resolution lattice image of Fig. 2(*D*) and its Fourier spectrum (Fig. 2*d*) can also be explained in terms of twin crystals. Fig. 5(*b*) shows atomic arrangements viewed from the [35$\bar{2}$] direction (black circles) and [1$\bar{1}$6] direction (red circles), both of which make angles of 56° with the (111) plane normal. The former produces 111 type diffraction spots (black filled circles) and the latter produces diffraction spots that constitute an orthogonal pattern (red filled circles). The $\bar{1}$11 spot produced by the former and the 220 spot produced by the latter have an interplanar angle of 57°. The extra spots shown by open squares in Fig. 5(*b*2) can occur by double diffraction through the two twin crystallites. The atomic arrangement and the diffraction pattern are in good agreement with the lattice image of Fig. 2(*D*) and its Fourier spectrum (Fig. 2*d*), respectively.

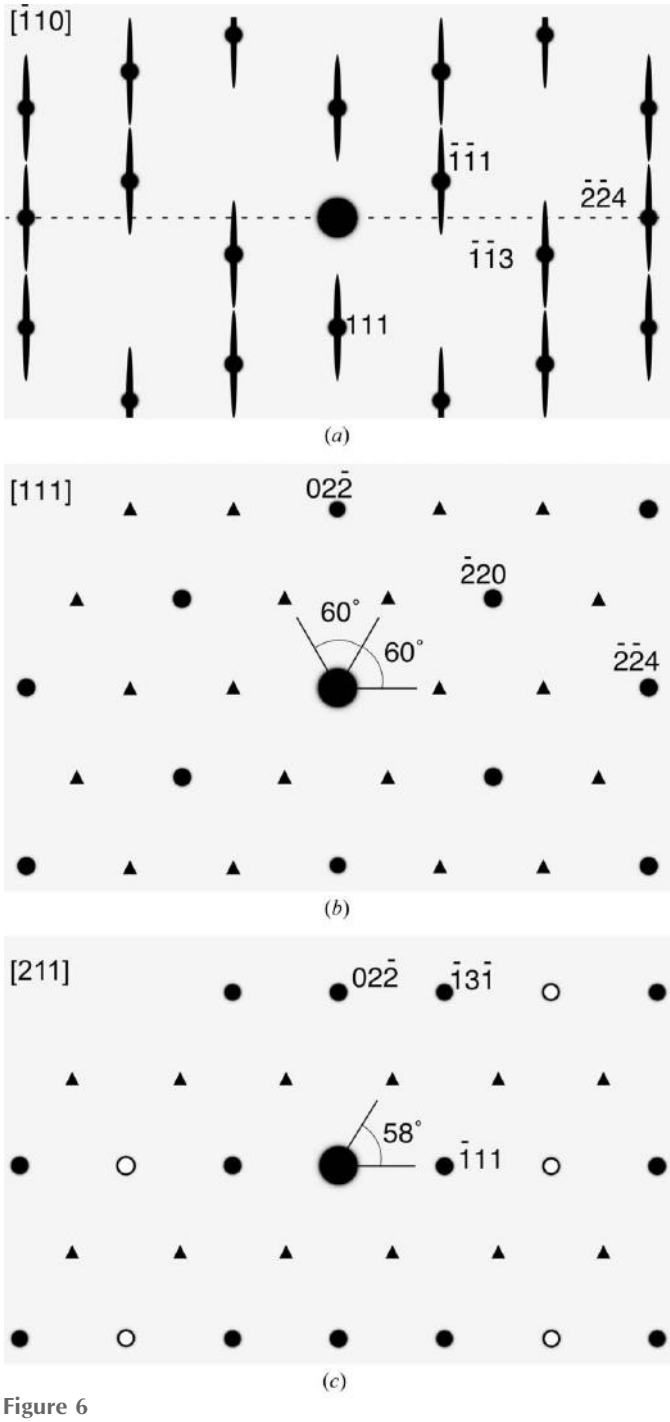

Figure 6
Electron diffraction patterns including extra spots caused by the streaking effect due to stacking faults parallel to (111): (*a*) [$\bar{1}$10], (*b*) [111] and (*c*) [211]. Filled circles indicate fundamental spots, and open circles and filled triangles indicate extra spots by double diffraction and the streaking effect, respectively.

Fig. 6(*a*) illustrates the streaking effect in the electron diffraction patterns from [$\bar{1}$10], which is perpendicular to the (111) twin boundary. The very limited thicknesses of the layered crystallites parallel to (111), which are due to twins and stacking faults, give rise to streaking in the [111] direction. When a large number of stacking faults on (111) are present, as observed in the high-resolution image of Fig. 3, the streaks are so much extended as to produce extra spots in the [111] pattern (Fig. 6*b*). The diffraction spots at $\frac{\bar{2}}{3}\ \frac{\bar{2}}{3}\ \frac{4}{3}$ and equivalent positions, shown by filled triangles, occur by elongation of $\bar{1}\bar{1}$1 type spots. These extra spots of sixfold symmetry are located at the positions corresponding to the {111} spacing of the diamond cubic structure and cannot be distinguished from those of 10$\bar{1}$0 type of the hexagonal structure, as shown in Fig. 4(*b*2). In the [211] diffraction pattern (Fig. 6*c*), streaking of $\bar{1}$1$\bar{1}$ type diffraction spots causes extra spots, such as $\frac{\bar{1}}{2}\ \frac{3}{2}\ \frac{\bar{1}}{2}$, shown by filled triangles. The extra $\frac{\bar{1}}{2}\ \frac{3}{2}\ \frac{\bar{1}}{2}$ spot and the standard $\bar{1}$11 spot have an interplanar angle of 58°, which is equal to the angle observed in Fig. 4(*a*1). The diffraction patterns of Figs. 6(*b*) and 6(*c*) are closely similar to the experimentally observed patterns of Figs. 4(*a*2) and 4(*a*1), respectively. The defective model with {111} twins explains very well the experimentally obtained electron diffraction patterns of crystalline particles: they can be understood as the superposition of diffraction patterns with elongation of the diffraction spots caused by twins and stacking faults on {111}.

4. Conclusion

We analysed the structure of the crystalline particles in sputter-deposited amorphous Ge by TEM. High-resolution TEM observations revealed that the coarse crystalline particles include a number of planar defects, namely stacking faults and twin boundaries parallel to {111}, and are composed of very thin layered crystallites, each of which contains fewer than ten (111) planes. The diffraction patterns taken from various crystallographic directions do not agree with those expected from hexagonal structures, but can be reproduced by assuming the defective cubic structure, by considering the following effects on electron diffraction patterns: superposition of the patterns from twin crystallites, double diffraction through them and streaking effects.

Acknowledgements

TEM observations were supported by Osaka University Microstructural Characterization Platform as the programme 'Nanotechnology Platform' of the Ministry of Education,

Culture, Sports, Science and Technology, Japan. We are grateful to Dr T. Sakata and Mr E. Taguchi for their technical support with TEM operations. The authors thank one of the referees of the original manuscript for helping them properly interpret the Fourier spectrum of Fig. 2(*d*).

Funding information

The following funding is acknowledged: JSPS KAKENHI (grant No. JP26420727; grant No. JP17J06339); The Murata Science Foundation (grant No. H28-58).

References

Buffat, P. A., Flüeli, M., Spycher, R., Stadelmann, P. & Borel, J. P. (1991). *Faraday Discuss.* **92**, 173–187.

Cayron, C., Den Hertog, M., Latu-Romain, L., Mouchet, C., Secouard, C., Rouviere, J.-L., Rouviere, E. & Simonato, J.-P. (2009). *J. Appl. Cryst.* **42**, 242–252.

Dickson, E. W. & Pashley, P. W. (1962). *Philos. Mag.* **7**, 1315–1321.

Hertog, M. I. den, Cayron, C., Gentile, P., Dhalluin, F., Oehler, F., Baron, T. & Rouviere, J. L. (2012). *Nanotechnology*, **23**, 025701.

Kohno, H., Ozaki, N., Yoshida, H., Tanaka, K. & Takeda, S. (2003). *Cryst. Res. Technol.* **38**, 1082–1086.

Matsuda, A. (2004). *J. Non-Cryst. Solids*, **338–340**, 1–12.

Okugawa, M., Nakamura, R., Ishimaru, M., Watanabe, K., Yasuda, H. & Numakura, H. (2016*a*). *J. Appl. Phys.* **119**, 214309.

Okugawa, M., Nakamura, R., Ishimaru, M., Yasuda, H. & Numakura, H. (2016*b*). *J. Appl. Phys.* **120**, 134308.

Okugawa, M., Nakamura, R., Ishimaru, M., Yasuda, H. & Numakura, H. (2016*c*). *AIP Adv.* **6**, 125035.

Parsons, J. R. & Hoelke, C. W. (1983). *Nature*, **301**, 591–592.

Parsons, J. R. & Hoelke, C. W. (1985). *Philos. Mag. A*, **50**, 329–337.

Poate, J. M. & Mayer, J. W. (1982). Editors. *Laser Annealing of Semiconductors.* New York: Academic Press.